

# Role of Sequence and Conformation on the Photochemistry and the Photophysics of A–T DNA Dimers: An Experimental and Computational Approach

Luis Colón,<sup>†,‡</sup> Carlos E. Crespo-Hernández,<sup>\*,§</sup> Rolando Oyola,<sup>||</sup> Carmelo García,<sup>||</sup> and Rafael Arce<sup>\*,†</sup>

Department of Chemistry, University of Puerto Rico, Río Piedras Campus, San Juan, Puerto Rico 00931, Department of Chemistry, The Ohio State University, Columbus, Ohio 43210, and Department of Chemistry, University of Puerto Rico, Humacao Campus, Humacao, Puerto Rico 00791

Received: January 12, 2006; In Final Form: May 2, 2006

The role of base sequence and conformation on the photochemistry and photophysics of thymidylyl (3'–5')–2'-deoxyadenosine sodium salt (TpdA) and 2-deoxyadenylyl (3'–5')–thymidine ammonium salt (dApT) was studied. To this end, nanosecond transient absorption at 266 nm, steady-state irradiation at 254 nm, and quantum chemical calculations were used. The transient absorption spectra show the solvated electron broad band in the visible region for each dinucleotide. In addition, low-intensity absorption bands are observed in the UV region, which are attributed to the deprotonated and protonated neutral radicals of adenine and thymine bases. Photoionization (PI) occurs by one- and two-photon pathways; the latter accounting for ~70% of the net PI yield. A diffusion-limited rate constant of  $2.0 \times 10^{10} \text{ M}^{-1} \text{ s}^{-1}$  was obtained for the reaction of the neutral molecule with the photoejected electron in both sequences. The photodestruction yield, measured from the chromophore loss at 260 nm, decreases in the presence of well-known electron scavengers. This suggests the participation of base radical anions as one of the photodegradation pathways, which is higher in TpdA than in dApT. The intermediacy of a radical ion pair (charge separated state) between the adjacent adenine and thymine bases is proposed in the formation of the [2 + 2] cycloadduct intermediate. The [2 + 2] cycloadduct intermediate is known to be the precursor of the thymine–adenine eight-member ring photoproduct (TA\*). Conformational constraints in the radical ion pair are suggested to explain the absence of the TA\* photoproduct in dApT. This hypothesis is supported by semiempirical calculations performed on all relevant reactive intermediates proposed to participate in the mechanism of formation of TA\*. Altogether, the results show that sequence and conformation profoundly influence the photochemistry and the photophysics of these DNA model systems.

## 1. Introduction

Long-range DNA-mediated charge transfer currently attracts considerable interest because of the key role played by oxidation in aging, mutagenesis, and carcinogenesis.<sup>1–16</sup> However, the influence that base sequence and conformation has on the photochemical and photophysical properties of DNA and its constituents has received much less attention.<sup>17–21</sup> In 1983, Davies and co-workers presented a classic example of the significant role of base sequence and conformation on the photochemistry of adjacent purine and pyrimidine bases in DNA.<sup>22–25</sup> The photoreaction of deoxyribo-dinucleoside monophosphate thymidylyl (3'–5')–2'-deoxyadenosine sodium salt (TpdA) at 254 nm, produced the thymine–adenine adduct as major photoproduct (TA\*). Significantly, this product was not detected in the photochemistry of its sequence isomer 2'-deoxyadenylyl (3'–5')–thymidine (dApT). Thus, the formation of the TA\* photoproduct can be considered as a sequence-specific intramolecular photoaddition. The biological significance of this lesion in DNA has been demonstrated by its

mutagenic properties in *Escherichia coli*<sup>26</sup> and by its possible contribution to the mutation spectrum of UV-irradiated plasmids.<sup>21,27,28</sup> The formation of TA\* photoproduct has also been observed in DNA oligonucleotides.<sup>28</sup>

Recently, Taylor and collaborators confirmed that TA\* consists of an eight-member ring product using NMR and molecular mechanics modeling.<sup>29</sup> The eight-member ring results from a fragmentation of the primary [2 + 2] cycloadduct, formed through the reaction of the 5,6 double bond of thymine and the six-member ring of the adenine moiety.<sup>29</sup> The singlet excited state was proposed as precursor of the TA\* photoproduct in TpdA because its formation is unaffected by triplet state quenchers such as O<sub>2</sub> and Mn<sup>2+</sup>.<sup>23</sup> In addition, triplet sensitization of TpdA with acetone did not form this product.<sup>23</sup>

Ballini et al. investigated the room-temperature photophysics of the sequence isomers TpdA and dApT in neutral aqueous solutions using synchrotron radiation with a time-correlated single photon counting detection system.<sup>30</sup> The fluorescence emission and excitation spectra were separated into two components with picosecond and nanosecond lifetimes, respectively. The picosecond spectrum was assigned to contributions from the mixed monomers (A and T) fluorescence and was ascribed to the unstacked fraction of the dinucleotides. However, recent experimental data show that adenine and thymine monomers in unstacked oligonucleotides decay in ultrafast time

\* To whom correspondence may be addressed: Rafael Arce, phone (787)-764-0000 X- 2433, fax (787)-759-6885, e-mail rarce@uprr.pr; Carlos E. Crespo-Hernández, e-mail ccrespo@chemistry.ohio-state.edu.

<sup>†</sup> University of Puerto Rico, Río Piedras Campus.

<sup>‡</sup> Deceased.

<sup>§</sup> The Ohio State University.

<sup>||</sup> University of Puerto Rico, Humacao Campus.

scales,<sup>31,32</sup> making such assignments dubious. Ballini and co-workers<sup>30</sup> assigned the long-lived emission components to emission from the vertically stacked bases. Different ground-state stacking conformations in both dinucleotides were suggested to account for the difference in population and relative intensities of the emitting states.<sup>30</sup> Because the vertically stacked excited state was more abundant in TpdA than in dApT, the authors proposed this state as the precursor of the TA\* photoproduct, accounting for the difference in photoreactivity.<sup>30</sup>

In this work, a comprehensive study of the photochemical reactivity of the T–A versus A–T sequence is presented from the perspective of the participating reactive intermediates and the photodestruction yields. This is a continuation of our research efforts to understand the role of sequence, base stacking, and conformation on the photochemistry and photophysics of DNA model compounds.<sup>20,33</sup> To this end, nanosecond laser flash transient absorption spectroscopy and steady-state photolysis studies were performed to investigate in detail the photochemistry and photophysics of TpdA and dApT dinucleotides at 298 K. In addition, the molecular and the electronic configurations of the ground and the excited singlet states were investigated for both dinucleotides using quantum chemical simulations. Calculations were also performed on the relevant reactive species proposed to be involved in the formation of TA\* photoproduct.

## 2. Material and Methods

**2.1. Chemicals and Sample Preparation.** Thymidylyl (3'–5')–2'-deoxyadenosine sodium salt and 2'-deoxyadenylyl (3'–5')–thymidine ammonium salt were used without further purification (Sigma Chemical Co.). Other chemical reagents were obtained from well-known suppliers. Samples were prepared by dissolving the dinucleotide in Nanopure water (Nanopure II, Barnstead). Aqueous solutions (pH 6.8) of the dinucleotide were used unless otherwise stated. Some samples were saturated with O<sub>2</sub>, N<sub>2</sub>O, N<sub>2</sub>, and Ar gases (Air Products, San Juan, PR) by continuously bubbling the corresponding gas through the solution using a stainless steel syringe inserted into the photolysis cell.

**2.2. Laser Irradiation Conditions and Data Analysis.** The transient absorption spectrokinetic system has been described elsewhere.<sup>34,35</sup> Briefly, a Continuum Surelite II Nd:YAG Q switched laser delivering up to 60 mJ at 266 nm was used as the excitation source. Time-resolved absorption measurements were made perpendicular to the excitation beam by using a conventional Xe 300-W arc lamp (Oriel Corp.), an Acton Research model 305 monochromator, and a R928 five-stage wired photomultiplier tube. The analyzed volume corresponded to the first few millimeters of the front cell exposed to the laser light. The signal was digitized with a LeCroy 9310A 400-MHz oscilloscope. A flow system was used for spectral acquisition to ensure that a fresh solution was irradiated at each laser pulse. The absorption of solutions was not allowed to decrease more than 15% during data acquisition to minimize any possible interference from photoproducts.

**2.3. Actinometry and Quantum Yields Determination.** The light fluence in the continuous photolysis at 254 nm was measured using the potassium ferrioxalate actinometer developed by Hatchard and Parker.<sup>36</sup> The quantum yields of photodestruction (in molecules/photon or mol einstein<sup>−1</sup>) were determined using the dosimetry method described by Johns,<sup>37</sup> as explained in detail elsewhere.<sup>38</sup> The concentration of the consumed dinucleotide was determined from the changes in the absorbance of the solutions at 260 nm. A static cell was used

for the determination of steady state quantum yields. However, solutions were continuously bubbled with a gas flow (N<sub>2</sub>, Ar, O<sub>2</sub>, or N<sub>2</sub>O) before (15 min) and during photolysis. Laser-induced electron photoejection yields were determined using KI as a reference ( $\varphi_e^- = 0.36$ )<sup>39</sup> at laser intensities of 5 and 10 MW/cm<sup>2</sup>, as described previously.<sup>20,33</sup>

**2.4. Quantum Chemical Calculations.** Geometry optimizations were performed with HyperChem 7.0 (HyperCube Inc., Florida) using a combination of molecular mechanics (MM+), molecular dynamics, and semiempirical calculations for closed shells (PM3/RHF/CI) and open shells (PM3/UHF), as described previously.<sup>34,35,40</sup> MM+ was used for initial optimization of all closed shell systems. To reduce the computation time, the optimized ground-state structures were used as the starting configuration for the first singlet-excited states (S1), which in turn were used as initial structures for all other excited species and intermediate radical cations. The optimization of the S1 state was performed using the RHF/half electron method. At the semiempirical level, the optimizations were done with the Polak-Ribiere conjugated gradient protocol ( $1 \times 10^{-5}$ ) convergence limit, 0.01 kcal/(Å mol) root mean square (rms) limit. The lowest energy conformations were found by randomly varying either the phosphate–CH<sub>2</sub> or the thymine–sugar torsion angle containing the N–glycosidic bond. The generation of a new starting conformation uses the “torsional flexing” motion of Kolossváry and Guida for energy minimization, which effectively leads to new ring conformations while avoiding large atomic displacements that can diminish the efficiency of optimization.<sup>41</sup> The structure of the [2 + 2] cycloadduct intermediate and the final TA\* product presented in Figure 5 were optimized using MM+ and the AMBER99 force field with a rms gradient of 0.003 kcal/(Å mol).

All molecular and spectroscopic parameters were obtained with PM3/RHF/CI-single point calculations starting from the most stable PM3-optimized conformation and using three occupied and three virtual orbitals. The gas-phase ionization potential (IP<sub>g</sub>) was either taken as the negative of the HOMO energy (Koopman's theorem) or calculated from the formation enthalpy of the molecule and the corresponding cation (IP<sub>g[X]</sub> =  $\Delta H_{f[X^+]} - \Delta H_{f[X]}$ ). Since Koopman's theorem is based on the assumption of a “vertical” ionization and, therefore, does not consider the stabilization of the system due to changes in the geometry of the cation radical, the latter method (“adiabatic” process) was used for further calculations. The photoionization energies presented in this work are in favorable agreement with those recently reported using ab initio methods for the DNA and RNA bases in gas phase and in aqueous solution.<sup>42</sup> Spin densities were obtained from the difference between  $\alpha$ - and  $\beta$ -electron populations.

## 3. Results and Discussion

**3.1. Transient Absorption Laser Flash Photolysis at 266 nm.** The transient absorption spectra of TpdA in a nitrogen-saturated aqueous solution, recorded at various delay times, are shown in Figure 1. The spectra consist of bands in the 290–360 and in the 400–750 nm wavelength regions. Similar spectra were obtained for dApT. Significantly, the dinucleotides do not show the triplet–triplet absorption band, neither crocetin sensitization of their excited triplet state was observed (data not shown). The visible broad band with maximum near 700 nm corresponds to the well-known spectrum of the solvated electron.<sup>39</sup> The decay rate of this band is strongly enhanced in the presence of oxygen, nitrous oxide, or at pH 2.0, supporting the assignment of this band to the hydrated electron absorption.

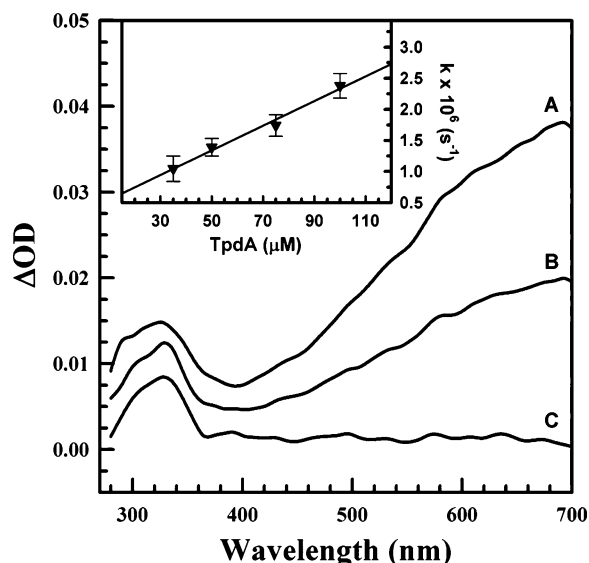


**Figure 1.** Transient absorption spectra recorded at (A) 96 ns, (B) 288 ns, and (C) 4.1  $\mu$ s delay times after 266 nm laser excitation of TpdA in nitrogen-saturated aqueous solution. Inset: kinetic rate constant at 700 nm as a function of TpdA concentration.

**SCHEME 1: Intermediate Species Produced after 266 nm High-Intensity and 254 nm Low-Intensity Excitation<sup>a</sup>**

$\text{TpdA} + h\nu \leftrightarrow {}^1(\text{TpdA})^*$ ; monomer and excimer emission/internal conversion

${}^1(\text{TpdA})^* \rightarrow \text{TpdA}^{\cdot+} + e^-$ ; one and two-photon ionization (I)

$\text{TpdA} + e^- \rightarrow \text{T}^{\cdot-}\text{pdA}$  or  $\text{TpdA}^{\cdot-}$ ; adenine and thymine electron adducts (II)

$\text{TpdA}^{\cdot+} + e^- \rightarrow \text{T}^{\cdot-}\text{pdA}^{\cdot+}$ ; fast electron trap by adjacent thymine (III)

${}^1(\text{TpdA})^* \rightarrow \text{T}^{(\delta-)}\text{pdA}^{(\delta+)}$ ; dark, charge transfer state (IV)

$\text{T}^{\cdot-}\text{pdA}^{\cdot+}$  and/or  $\text{T}^{(\delta-)}\text{pdA}^{(\delta+)} \rightarrow [2 + 2]$  cycloadduct (V)

$\text{T}^{\cdot-}\text{pdA}^{\cdot+}$  and/or  $\text{T}^{(\delta-)}\text{pdA}^{(\delta+)} \rightarrow \text{TpdA}$ ; charge recombination

<sup>a</sup> Dinucleotide neutral radicals and OH adducts are not shown. See text for discussion

The prompt appearance of the solvated electron absorption (faster than the response time of our kinetic spectrometer) shows that excitation with 266 nm laser pulses induce photoionization of the dinucleotides (DNPs) in the subnanosecond time scales (Scheme 1, I). The hydrated electron disappears with a pseudo-first-order kinetics. A plot of the pseudo-first-order rate constant as a function of the initial ground-state concentration resulted in a line with slope of  $2.0 \times 10^{10} \text{ M}^{-1} \text{ s}^{-1}$  for both dinucleotides (Figure 1, inset). This value is typical of diffusion-controlled reactions, as observed for the reaction of the DNA bases with the solvated electrons.<sup>43</sup> Thus, one of the pathways for electron decay in these dinucleotides is the formation of electron adducts (II).

Further evidence that the dinucleotides radical anions contribute to the UV transient absorption band was obtained from competition experiments using known electron scavengers. The slow decay of the UV band ( $\tau > 15 \mu$ s) in  $\text{N}_2$ -saturated solutions is significantly reduced in the presence of known electron

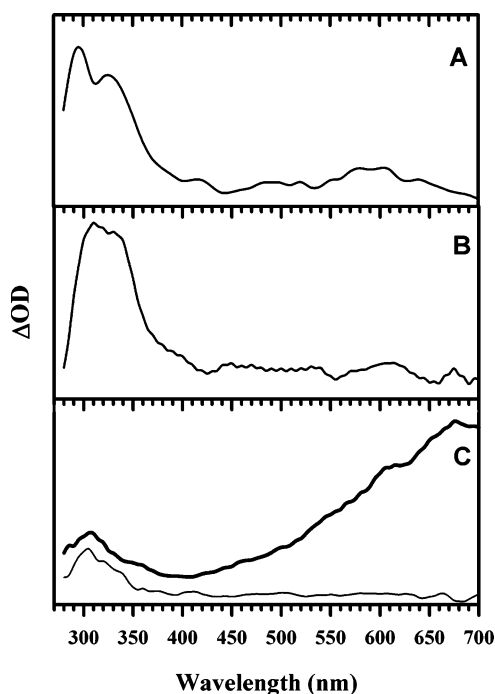


**Figure 2.** Transient absorption spectra of TpdA recorded at (a) 150 ns after 266 nm laser excitation in  $\text{N}_2\text{O}$ -saturated aqueous solution and the presence of 0.5 M *tert*-butyl alcohol, (b) 15  $\mu$ s after 266 nm laser excitation in nitrogen-saturated solution at pH = 2.0, and (c) 192 ns (thick) and 14  $\mu$ s (thin) after 266 nm laser excitation in nitrogen-saturated solution at pH = 12.0.

scavengers. For example, a 50% reduction of the intensity of the UV band was observed in  $\text{N}_2\text{O}$  saturated solutions containing 0.5 M *tert*-butyl alcohol (Figure 2A), relative to the absorption in nitrogen-saturated solution. Here, *tert*-butyl alcohol is used to scavenge OH radicals, which are produced by the reaction of  $\text{N}_2\text{O}$  with the hydrated electrons. Similarly, the initial absorbance at 330 nm decreases by 75% or 30% in the presence of air ( $\text{O}_2$ ) or acid pH, respectively (Figure 2B). In addition, only the radical anions of the dinucleotides and the hydrated electron are observed at basic pH conditions ( $\text{N}_2$ -saturated aqueous solution and pH 12). The UV absorption band in basic pH is in the same wavelength region as that observed at neutral pH (Figure 2C). Thus, the UV band at neutral pH has contributions from the absorption of the radical cations and anions of the bases (I and II). These radical cations and anions are readily present as neutral radicals in our nanosecond transient absorption studies due to their fast deprotonation and protonation, respectively, in neutral aqueous solutions.<sup>43</sup> Quantum chemical calculations predict that the absorption band of these radical should appear in this UV region, in agreement with the experiments (vide infra).

The participation of the protonated radical anions is also supported by the reported spectra of the electron adducts for the monomeric units and their corresponding protonated neutral radicals. These radicals absorb at similar wavelength regions than those shown in Figure 2. The thymine electron adduct shows an absorption band below 310 nm with maximum around 300 nm. It undergoes rapid protonation at C2, C4, C5, and C6, forming neutral radicals with absorption maxima at 305, 330, 390, and 385 nm, respectively.<sup>44,45</sup> The electron adducts of the adenine nucleoside (dAdo) and nucleotide (dAMP), and their corresponding protonated radicals, have also been characterized by pulse radiolysis and laser photolysis studies.<sup>46</sup> The adenine neutral radicals have been identified as  $\text{A}(\text{C8H})^*$ ,  $\text{A}(\text{NH})^*$ , and



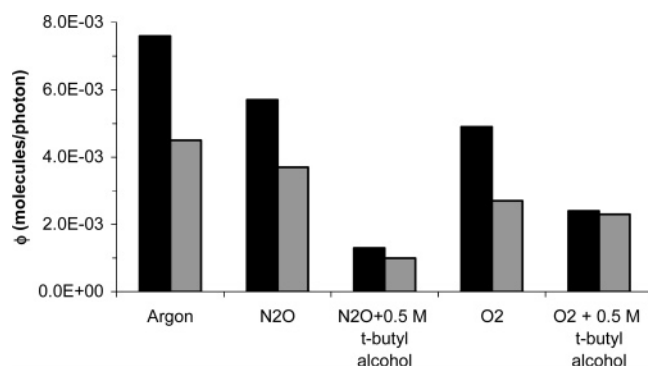


**Figure 3.** Photodestruction quantum yields (molecules/photon) of TpdA (black) and dApT (gray) under different experimental conditions.

A(C2H)<sup>•</sup>, with absorption maxima at 310, 315, and 355 nm, respectively.<sup>46</sup>

**3.2. Hydrated Electron Yield and Its Dependence on Laser Intensity.** The absorbance at 720 nm, measured 50 ns after the laser pulse, increases in a quasi-linear form with an increase in laser power (data not shown). The dependence of the transient absorption signal on the laser intensity was further analyzed using eq 1

$$\frac{A}{I} = \alpha + \beta I \quad (1)$$

where  $A$  is the absorbance at 720 nm,  $I$  is the laser intensity in W/cm<sup>2</sup>,  $\alpha$  is a coefficient related to the quantum yield of the one-photon processes, and  $\beta$  is a factor that depends on the molar absorption coefficients and yields of the intermediate species in the consecutive two-photon process.<sup>47–49</sup> The net photoionization (PI) yields for dApT and TpdA at 5 MW/cm<sup>2</sup> are 0.038 and 0.030, respectively. The monophotonic component contributes only ~25 and 33% to the net PI yield of dApT and TpdA, respectively. Changes in base stacking overlap and conformation have been suggested to explain the different net PI yields in these dinucleotides.<sup>20,33</sup>

**3.3. Determination of Photodestruction Quantum Yields Using Low-Intensity 254 nm Irradiation.** The photodestruction quantum yield was studied under different experimental conditions. The yields were determined at low photoconversion efficiency to avoid interferences from the formation of absorbing photoproducts. Figure 3 shows the yields in the presence or absence of electron scavengers for each dinucleotide. Importantly, the differences observed in the yields are directly related to conformational differences in these dinucleotides because all other experimental parameters were kept constant. Strikingly, the photodestruction yield is 1.7-fold higher yield for TpdA than for dApT (Figure 3) in Ar-saturated solutions, i.e.,  $(7.6 \pm 0.4) \times 10^{-3}$  vs  $(4.5 \pm 0.3) \times 10^{-3}$  molecules/photon, respectively. The higher yield has a contribution from the selective formation of TA\* in TpdA. However, the difference in yield ( $\Delta\phi = 3.1 \times 10^{-3}$ ) cannot only be attributed to the formation of TA\* because its quantum yield is  $7 \times 10^{-4}$ .<sup>25</sup> Thus, there must be other photoproducts formed in higher yield in TpdA than in dApT. These results show that DNA base sequence significantly affects their photoreactivity, in agreement with results reported by Livneh et al.<sup>19</sup> and by our group for the GC dimer isomers.<sup>20</sup>

Oxygen (O<sub>2</sub>) and N<sub>2</sub>O are efficient electron scavengers with rate constants of  $1.88 \times 10^{10} \text{ M}^{-1} \text{ s}^{-1}$  and  $8.7 \times 10^9 \text{ M}^{-1} \text{ s}^{-1}$ , respectively.<sup>50</sup> The photodestruction yield for TpdA and dApT in O<sub>2</sub>-saturated conditions is  $(4.9 \pm 0.4) \times 10^{-3}$  and  $(2.7 \pm 0.4) \times 10^{-3}$ , respectively. In N<sub>2</sub>O-saturated conditions, the yield

is  $(5.7 \pm 0.3) \times 10^{-3}$  and  $(3.7 \pm 0.3) \times 10^{-3}$  for TpdA and dApT, respectively. Thus, the photodestruction yield of TpdA decreases by 25% and 36% in the presence of N<sub>2</sub>O and O<sub>2</sub> and that of dApT by 18% or 40%, respectively, relative to Ar- or N<sub>2</sub>-saturated solutions. The effect of the electron scavengers on the yields indicates that the hydrated electrons participate in the degradation of the DNPs through pathways I and II (Scheme 1). This is in good agreement with the observed change in intensity in the transient absorption measurements of the dinucleotides in the presence of electron scavengers (section 3.1).

Scavenging of electrons by O<sub>2</sub> and N<sub>2</sub>O can generate OH radicals, which are known to react efficiently with the DNA bases through oxidation and addition reactions.<sup>51–56</sup> Thus, steady-state photolysis experiments were also performed in the presence of *tert*-butyl alcohol to test the participation of OH radicals in the photodestruction mechanism of the dinucleotides (Figure 3). Solutions of irradiated TpdA, containing 0.5 M *tert*-butyl alcohol and saturated with N<sub>2</sub>O or O<sub>2</sub>, resulted in a reduction of the photodestruction yields by 83% and 68%, relative to N<sub>2</sub>O- and O<sub>2</sub>-saturated solutions, respectively. Reductions of 78% and 49% were observed for dApT under similar conditions, respectively. These results suggest a significant participation of the OH radicals in the photodestruction mechanism of the dinucleotides in the presence of N<sub>2</sub>O and O<sub>2</sub> saturated conditions. The different percent of OH radical participation in the photodestruction yield ( $\Delta\phi_{\text{dest}} = 14\%$ ) can be attributed to conformational differences of these DNPs, which can modulate their reactivity toward OH radical attack. Similar sequence effects have been observed for the reaction of ketyl radicals and dinucleotides.<sup>19</sup>

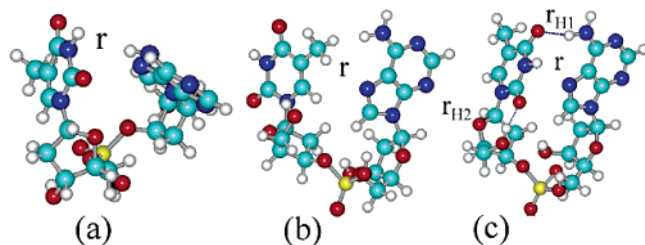
**3.4. Quantum Chemical Calculations.** Semiempirical PM3 calculations predict more than 20 conformations for each dinucleotide. This is in agreement with the results obtained by Gidzen and Bowers.<sup>57</sup> These authors reported the gas phase conformational and energetic properties of deprotonated dTA- and dAT- using ion-mobility and molecular modeling calculations at 80 K.<sup>57</sup> Their results provided evidence for the conformational differences between these two dinucleotides. The PM3-theoretical calculations performed in this work predict three different families of conformations for each sequence. Using Gidzen's nomenclature,<sup>57</sup> the most stable conformations are those stacked, followed by the base-paired conformations with one or two hydrogen bonds ("H-bonded" conformations) and then by the unstacked or open conformations. The stacked and "H-bonded" conformations were obtained when the conformational search was done varying the dihedral angle at the N-glycosidic bond. The unstacked conformations, on the other hand, required variations of the phosphate-CH<sub>2</sub> torsion angle.

Table 1 shows the calculated structural parameters of the three most stable conformations of each dinucleotide (see also Figure 4). The two most stable conformations are stacked, with geometries similar to those found in A- and B-like DNA conformations. The base stacking interactions are stronger for the TpdA than for the dApT conformers based on the interchromophore distance (Table 1). In addition, the majority of the "H-bonded" conformations have two H-bonds (Figure 4c, for instance). The third most stable conformation of dApT has a Watson-Crick-type H-bond between the adenine/NH<sub>2</sub> and the thymine/C=O ( $r_{\text{H}_1} = 2.84 \text{ \AA}$ ) and another between the phosphate and the sugar/OH ( $r_{\text{H}_2} = 3.02 \text{ \AA}$ ). The corresponding TpdA conformations have the same Watson-Crick-type bond ( $r_{\text{H}_1} = 1.85 \text{ \AA}$ ) and another one between the thymine/C=O and the sugar/OH ( $r_{\text{H}_2} = 1.81 \text{ \AA}$ ) (see Figure 4C). The standard bond

**TABLE 1: Theoretical Parameters of the Three Most Stable Conformations of the Dinucleotides in the Ground and the First-Excited States**

species	conformation	$\Delta H_f$ (kcal/mol)	$r^a$ (Å)	torsion angle (deg)		H bonds
				$b$	$c$	
dApT_S0	1	-417.25	6.6	-85.08	-66.2	0
	2	-416.14	6.9	-151.7	-72.9	0
	3	-415.33	6.2	-102	-67.3	2 <sup>d</sup>
dApT_S1	1	-317.78	6.7	-83.12	-55.9	0
	2	-317.49	6.9	-151.6	-73.4	0
	3	-317.39	6.2	-101.1	-67.7	2 <sup>d</sup>
TpdA_S0	1	-417.7	5.2	-85.2	143.7	0
	2	-417.19	5.6	-107.7	144.5	0
	3	-414.52	5	65.94	147.4	2 <sup>e</sup>
TpdA_S1	1	-318.86	5	-140.7	146.9	0
	2	-318.41	5.6	-83.14	143.5	0
	3	-316.3	5.5	64.14	146.9	2 <sup>e</sup>

<sup>a</sup> Distance between the C-CH<sub>3</sub> of thymine and the C-NH<sub>2</sub> of adenine. <sup>b</sup> Torsion angle of the glycosyl bond in thymidine measured between the bonds thymine/OC-NC...sugar/CH-OC. <sup>c</sup> Torsion angle for the thymidine-phosphate plane measured in the direction of the sugar oxygen. <sup>d</sup> Hydrogen bonds are between the adenine/NH<sub>2</sub>...thymine/C=O and between the phosphate...chain/CH<sub>2</sub>OH. <sup>e</sup> Hydrogen bonds are between the adenine/NH<sub>2</sub>...thymine/C=O and between the thymine/C=O...sugar/CH<sub>2</sub>OH.



**Figure 4.** PM3 conformations of (a) syn/anti dApT\_S0(1) with  $r = 6.62$  Å, (b) anti/anti TpdA\_S0(1) with  $r = 5.2$  Å, and (c) anti/anti TpdA\_S0(3) with  $r = 5.0$  Å.  $r_{H1} = 1.85$  Å and  $r_{H2} = 1.81$  Å.

distance for the adenine/NH<sub>2</sub>...thymine/C=O Watson-Crick bond in double-stranded DNA is 2.82 Å. This indicates that the H-bonded conformation of dApT has standard H-bonds, whereas that of dTpA has stronger bonds.

The optimized excited singlet state of the three more stable conformations was also determined using the half electron method. Relevant structural parameters are presented in Table 1 (see also Figure 6). The structural properties of the [2 + 2] cycloadducts and the trans-syn and cis-syn eight-member ring products are listed in Table 3. The ground and singlet excited states of TpdA are slightly more stable than those of the dApT conformers ( $\Delta\Delta H < 2$  kcal/mol, Table 1). However, an equal singlet state energy is predicted for both dinucleotides (~99 kcal/mol). The ground and singlet excited states show significant differences in the torsion angles of the thymine/OC-NC and sugar/CHOC planes and on the distance between the reactive centers of C-CH<sub>3</sub> in thymine and C-NH<sub>2</sub> in adenine (Table 1). For instance, the distance between the C-CH<sub>3</sub> of thymine and the C-NH<sub>2</sub> of adenine is at least 1.0 Å smaller for the TpdA conformers than for those of dApT.

Table 2 shows the spectroscopic properties of the TpdA and the dApT sequences, their monomeric components, and relevant reactive species. The reactive intermediates of dApT are not shown because the interest is in the species that might participate in the formation of the TA\* product. Base stacking in TpdA and in dApT sequences stabilize the bases by at least 190 and 340 kcal/mol, respectively. The radical cation of TpdA is predicted to absorb at wavelengths longer than 350 nm, whereas

the radical anion absorbs more strongly at  $\lambda \approx 290$  nm. The deprotonated neutral radicals have maximum absorbance between 280 and ~300 nm, whereas the protonated neutral radicals absorb strongly at ~270 nm. Although PM3 calculations of open shell species are not always reliable due to spin contamination with higher spin states, the calculations compared fairly well with the transient absorption bands reported in this work (Figures 1 and 2).

In section 3.1 it was suggested that it is not straightforward to determine from the transient spectra of the dinucleotides the relative contribution of each base to the net PI yield. This is due to the overlap of the absorption spectrum of the radical species produced after PI of adenine or thymine. Table 2 shows that protonated and deprotonated neutral radicals have absorption bands in the ~270–400 nm range. However, the quantum chemical calculations suggest that the adenine base contributes more to the photoionization of the dinucleotides (Table 4). This is in agreement with the redox properties of adenine and thymine,<sup>58,59</sup> and with spin corrected ab initio calculations of the first ionization energy for thymine and adenine bases in aqueous solution.<sup>42</sup> Furthermore, 80% of the electron density is localized in the adenine HOMO in each dinucleotide (Figure 6) and only the adenine base is responsible for the short wavelength excitations. In dApT, the 253 nm absorption corresponds to the HOMO-2 to LUMO+1 transition, whereas for TpdA the 252 nm absorption corresponds to the HOMO-2 to LUMO transition. Therefore, these bands correlate with the excitation band on the adenine nucleoside (Table 2). The long wavelength excitations include molecular orbitals in thymine or in both bases. In dApT, the absorption at 281 nm corresponds to a thymine-centered transition from HOMO-1 to LUMO+2. In TpdA, the absorption at 278 nm belongs to a combination of an adenine-centered transition from the HOMO to the LUMO and a thymine-centered transition from HOMO-1 to LUMO+1. Overall, the excitation initially involves adenine electrons in both dinucleotides.

**3.5. TA\* Photoproduct.** Even though the TA\* photoproduct was reported almost 20 years ago,<sup>25</sup> there is still a need of fundamental information on the reactive intermediate species participating in its formation. TA\* is a minor product in DNA, almost 2 orders of magnitude lower than the (6-4) photoadducts or the pyrimidine photodimerization.<sup>23</sup> Nonetheless, it has been proposed that its formation might be relevant at the cellular level because the TATA sequence is highly conservative in DNA.<sup>25,60</sup> Ballini et al. proposed a long-lived excited state of TpdA as the precursor of the TA\* photoproduct because its population in TpdA is almost twice that in dApT.<sup>30</sup> For this proposal to be valid, however, a TA\* quantum yield of  $\sim 3.5 \times 10^{-4}$  should be observed in dApT because its quantum yield in TpdA is approximately  $7 \times 10^{-4}$ .<sup>25</sup> Significantly, the TA\* photoproduct is not observed in dApT. Thus, the reactive precursor of the [2 + 2] cycloadduct intermediate (V, Scheme 1) is still under debate.

The formation of TA\* does not correlate with the reactive pathways I and II (Scheme 1). This is because a similar decrease in the transient UV absorption band (section 3.1) and in the photodestruction yield (section 3.3) was observed for both dinucleotides in the presence of N<sub>2</sub>O or O<sub>2</sub>. This observation also holds true in the presence of *tert*-butyl alcohol for the N<sub>2</sub>O- or O<sub>2</sub>-saturated experiments, ruling out the participation of OH radical attack in the formation of the TA\* product.<sup>61</sup> The observation of one- and two-photon ionization (I, in Scheme 1) in our transient absorption experiments suggests the intermediacy of a radical ion pair (charge separated state) of TpdA

**TABLE 2: Spectroscopic Properties of Adenine, Thymine (Thy), Their Nucleosides and Dinucleotides, the Most Stable Conformers of the Dinucleotides, and Their Corresponding Radicals**

species	$\Delta H_f$ (kcal/mol)	$r^a$ (Å)	torsion angle <sup>b</sup> (deg)	$\lambda$ (nm) [oscillator strength]
adenine	55.8			221 [1.00], 232 [0.84]
thymine	-76.7			221 [0.29], 230 [0.21], 243 [0.13], 302 [0.21]
adenosine	-73.1			223 [1.10], 232 [0.86], 295 [0.48]
Thy	-202.7			219 [0.40], 231 [0.33], 239 [0.17], 287 [0.13], 304 [0.09]
dApT_S0	-415.3	6.6	-66.22	253 [0.41], 281 [0.69], 295 [0.48]
TpdA_S0	-417.3	5.2	143.69	252 [0.41], 278 [1.06], 301 [0.17]
TpdA <sup>•+</sup>	-233.7	4.6	141.95	355 [0.22], 407 [0.32]
TpdA <sup>•-</sup>	-450.0	4.6	153.98	274 [0.42], 286 [0.57], 356 [0.18] <sup>c</sup>
TpdA <sup>•</sup> (1) <sup>d</sup>	-382.7	5.0	147.45	254 [0.28] <sup>e</sup> , 297 [0.64], 423 [0.10]
TpdA <sup>•</sup> (2) <sup>d</sup>	-363.5	5.1	146.65	280 [0.92], 299 [0.24]
TpdA <sup>•</sup> (3) <sup>d</sup>	-366.5	5	147.23	282 [0.61], 383 [0.15]
TpdA <sup>•</sup> (4) <sup>d</sup>	-401.8	5.0	147.56	267 [0.99], 285 [0.11], 368 [0.21]
TpdA <sup>•</sup> (5) <sup>d</sup>	-378.9	5.1	143.38	279 [0.57], 292 [0.41], 352 [0.11] <sup>f</sup> , 435 [0.69] <sup>g</sup>

<sup>a</sup> Distance between the C-CH<sub>3</sub> of thymine and the C-NH<sub>2</sub> of adenine. <sup>b</sup> Torsion angle for the thymidine-phosphate plane measured in the direction of the sugar oxygen. <sup>c</sup> Spin multiplicity = 2.34. <sup>d</sup> Neutral radicals formed when the radical cation is deprotonated at the thymine/CH<sub>3</sub> (1), at the thymine/NH (2), or the adenine/NH<sub>2</sub> (3) and when the radical anion is protonated at the adenine/NH (4) or at the thymine/NH (5). <sup>e</sup> Spin multiplicity = 2.13. <sup>f</sup> Spin multiplicity = 2.87. <sup>g</sup> Spin multiplicity = 2.68.

**TABLE 3: PM3 Calculated Physical Properties for the [2 + 2] Cycloaddition Intermediates and the Corresponding Final Products**

compound	$\Delta H_f$ (kcal/mol)	torsion angle (deg)	
		<i>a</i>	<i>b</i>
[2 + 2] trans-syn	-380.9	14.4	21.16
TA* trans-syn	-390.97	-173.06	47.62
[2 + 2] cis-syn	-382.94	15.27	4.21
TA* cis-syn	-391.16	-170.94	38.35

<sup>a</sup> Measured for the adenine (NH<sub>2</sub>-C-C-N). <sup>b</sup> Measured for the thymine (CH<sub>3</sub>-C-C-H).

**TABLE 4: Ionization Energies for the Three Most Stable Conformations of the Dinucleotides, the Corresponding Nucleosides, Thymine (Thy) and Adenine in Water ( $\epsilon = 78.5$  D)**

molecule	volume (Å <sup>3</sup> )	IE <sub>gas</sub> (eV)		IE <sub>aqueous</sub> (eV) <sup>c</sup>
		vertical <sup>a</sup>	adiabatic <sup>b</sup>	
adenine	415.6	8.84	8.22	5.38
thymine	396.6	9.53	8.89	6.03
adenosine	699.82	8.77	7.99	5.40
Thy	665.89	9.40	8.41	5.80
dApT (1) <sup>d</sup>	1304.35	8.59	8.50	6.15
dApT (2)	1316.11	8.83	8.46	6.11
dApT (3)	1288.66	8.64	7.61	5.26
TpdA (1)	1283.88	8.94	7.98	5.63
TpdA (2)	1298.09	8.93	7.96	5.61
TpdA (3)	1274.07	8.64	7.89	5.53

<sup>a</sup> Obtained from Koopman's theorem. <sup>b</sup> Calculated from the formation enthalpy of the molecule and the corresponding cation radical, i.e., IP =  $[(\Delta H_{\text{cation}} - \Delta H_{\text{neutral}})/23.05]$ . <sup>c</sup> Calculated from the "adiabatic" gas ionization potential. <sup>d</sup> Numbers refer to the conformation in Table 1.

in the formation of TA\*. This radical pair can be formed as result of adenine photoionization followed by fast electron trap by thymine before the electron can escape the TpdA cage (**III**, in Scheme 1). In other words, there is no need for diffusional encounter between thymine and the adenine-ejected electron in the dinucleotide.

Alternatively, the initial step of TA\* formation might arise from a dark (in emission), charge transfer state (**IV**), formed between vertically stacked adenine and thymine bases.<sup>31</sup> Specifically, we argue that the formation of a radical ion pair (**III** and/or **IV**) could be a likely precursor of the [2 + 2] cycloadduct intermediate (**V**, in Figure 5), from which the eight-member ring TA\* photoproduct is formed due to aromatic stabilization of the imidazole ring (Figure 5). The formation of **V** from **III**

and/or **IV** must compete with charge recombination<sup>31</sup> and protonation and deprotonation reactions leading to neutral radicals (see section 3.1). Cycloaddition reactions between a radical cation and a radical anion have been previously proposed in the formation of the trans-anti thymine dimer,<sup>62</sup> supporting our hypothesis.

We note that the transient absorption experiments presented in this work cannot provide direct evidence of the participation of **III** and **IV** in the DNPs photochemistry. Nonetheless, our quantum chemical calculations (Tables 1–4 and Figures 4–6) and recent femtosecond transient absorption experiments in AT-oligonucleotides<sup>31,63</sup> provide support to our hypothesis. Further support of the intermediacy of a charge separated or radical pair state in the formation of TA\* comes from photochemical experiments in TpdI and 5-methyl-CpdA dinucleotides.<sup>22</sup> The TpdI dinucleotide, where adenine has been replaced by inosine, also form an eight-member ring TI\* photoproduct (an analogue of TA\*), whereas 5-methylCpdA does not.<sup>22</sup> This suggests the participation of a radical ion pair as a precursor of TA\* and TI\*. In TpdI and TpdA dinucleotides, the driving force for charge separation is similar ( $E_{\text{ox}}(\text{A}) = 1.42$  V versus  $E_{\text{ox}}(\text{I}) = 1.40$  V),<sup>6,58</sup> but smaller in 5-methylCpdA.<sup>64</sup> As argued below, however, not only the probability of charge separation but the specific conformation of the dinucleotide at the time of excitation should play an important role in the formation of TA\* photoproduct.

It has been suggested that the TA\* product arises from an anti/anti glycosyl conformation of the nucleotides, as in B-form DNA conformation.<sup>29</sup> This seems to be in agreement with our quantum chemical calculations, which predict that the anti/anti glycosyl conformation is not present, or is present in very low yields, in dApT. However, our calculations also show that the anti/anti conformation does not play a major role in the TpdA isomer. The most stable dApT conformations are in anti/syn configuration for the ground state, the single excited state, and for its radicals (Table 1). The oxygen of the thymidine sugar is directed toward the adenosine moiety in all these conformations (Figure 4a). Similar anti/syn conformers are found in TpdA, as shown by the two most stable conformations in Table 1. Only the third conformer is in an anti/anti configuration (angle > 0). The distinction is that for TpdA the sugar is now oriented toward the outside of the dinucleotide (parts b and c of Figure 4). There is no net rotation around this thymidine glycosidic bond because of the change in orientation of the sugar.

The base orientation relative to the sugar in **III** and **IV**, and



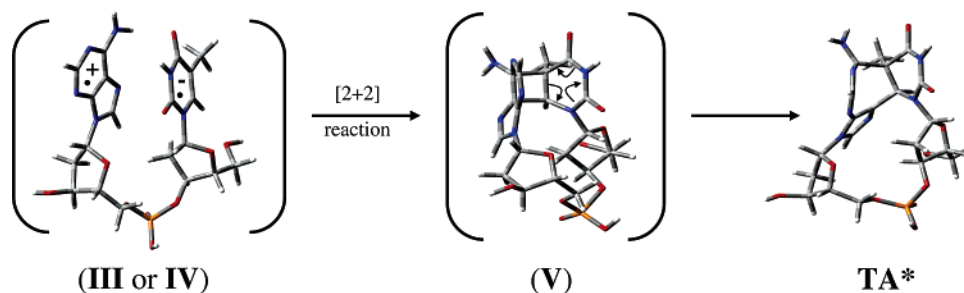


**Figure 5.** The proposed intermediacy of the A–T radical ion pair **III** or **IV** in the formation of the intermediate of the [2 + 2] cycloadduct **V**, through which the TA\* product is formed. Optimizations were performed using AMBER99 force field with a rms gradient of 0.003 kcal/(Å mol).

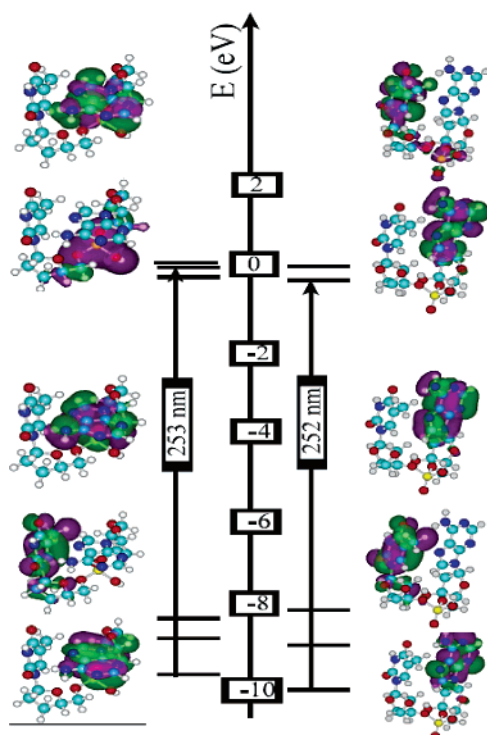


**Figure 6.** Molecular orbitals involved in the UV excitation of dApT (left) and TpdA (right) dinucleotides. For dApT, the LUMO+2 orbital ( $E = -0.26$  eV) is also involved (not shown) in the electronic transitions with  $\lambda = 281$  nm.

in the excited singlet state of the stacked bases, is not the major factor limiting the formation of the intermediate [2 + 2] cycloadduct (**V**). The TA\* photoadduct is not formed in dApT because the whole thymidine moiety is not favorably oriented toward the adenosine nucleoside. In the most stable dApT conformation, the thymidine moiety must rotate about 80° to achieve the corresponding lowest energy conformation in TpdA. This suggests that the distance between the double bonds in the radical ion pair, proposed to be involved in the formation of the [2 + 2] cycloadduct intermediate, to be longer in the dApT dinucleotide than in TpdA ( $r \sim 7\text{--}6.2$  Å vs  $r \sim 5\text{--}5.6$  Å, respectively, Table 1). Furthermore, this increase in distance is more pronounced in the excited state of the stacked dApT isomer, making the formation of the [2 + 2] cycloadduct even less favorable. In this regard, the charge recombination in AT-alternated oligonucleotides occurs in  $\sim 50$  ps.<sup>31</sup> Thus, charge recombination should compete efficiently with the formation of the TA\* product. The observation that the photoionization yield is similar for both dinucleotides but that only TpdA forms the TA\* product might also be explained by the unfavorable conformation of dApT, which does not allow formation of the [2+2] cycloadduct intermediate. This is because for TpdA, on the other hand,  $r < 5.5$  Å and decreases upon excitation for

two of the three most stable conformations found in our PM3 calculations (parts b and c of Figure 4). The molecular orbitals involved in the electronic excitations in TpdA\_S1(1) conformation are in a better configuration to favor cross addition (Table 1 and Figure 6).

In summary, quantum chemical calculations suggest that the determining factor in the formation of TA\* is the specific orientation of the base-stacked adenine and thymine bases (base–base overlap) in the anti/syn conformation for the precursors **III** and/or **IV**. This orientation is related to the alignment of the thymidine sugar in the DNPs. Additionally, the formation of **V** from **III** and/or **IV** must compete with charge recombination, and protonation and deprotonation reactions leading to neutral radicals. In this sense, the actual conformation of ApdT at the time of excitation controls whether the charge-separated state (**III** and/or **IV**) form or not the [2+2] cycloadduct intermediate. In this regard, the low quantum yield of TA\* product in DNA compared to TpdA<sup>23–25</sup> could be a consequence of conformational constraints imposed by the base-pairing interactions in the polymer. Studies of DNA components in solution have shown that microenvironment factors such as viscosity and ionic strength modulate the conformation and dynamics of DNA.<sup>65–68</sup> There is also evidence for the existence and coexistence of a variety of conformations of A/T and T/A oligomers, both in gas and in aqueous phases,<sup>17,30,57,68–70</sup> leading to a different orbital overlap of the stacked bases. However, a detailed description of the conformations, with particular attention to base overlap geometry and population distribution is not available for aqueous solutions of TpdA or dApT. This structural information must be obtained before further discussion is warranted. We note that picosecond infrared transient absorption spectroscopy<sup>71</sup> is a suitable technique to obtain “real time” structural/mechanistic information on the intermediate species leading to TA\* product formation and potentially of other DNA photoreactions.

#### 4. Conclusion

In this work, we show that sequence and conformational differences profoundly influence the photochemistry and photophysics of TpdA and dApT dinucleotides. The formation of the radical ion pairs **III** and/or **IV** is proposed as a plausible intermediate species in the formation of the [2 + 2] cycloadduct **V**, from which the TA\* product is formed. The formation of **V** from the radical pair must compete with charge recombination and protonation and deprotonation reactions leading to the formation of neutral radicals. Conformational constraints on the singlet excited state and on the radical ion pair are suggested to explain the absence of the TA\* product in dApT. This hypothesis is supported by semiempirical calculations performed on all relevant species proposed to be involved in the mechanism of formation of TA\* and observed in transient absorption experiments.

**Acknowledgment.** This article is dedicated to the memory of Luis Colón. This work has been supported in part by NIH-MBRS Grants S06GM08216, 08102 and from the Research Centers on Minority Institutions award RR-03641 (Division of Research Resources NIH). R. Oyola also appreciates the financial support from GAAN fellowship program from the Department of Education, USA, and the Puerto Rico Industrial Development Company.

## References and Notes

- (1) Wan, C. Z.; Fiebig, T.; Schiemann, O.; Barton, J. K.; Zewail, A. H. *Proc. Natl. Acad. Sci. U.S.A.* **2000**, *97*, 14052–14055.
- (2) Douki, T.; Angelov, D.; Cadet, J. *J. Am. Chem. Soc.* **2001**, *123*, 11360–11366.
- (3) Wan, C. Z.; Fiebig, T.; Kelley, S. O.; Treadway, C. R.; Barton, J. K.; Zewail, A. H. *Proc. Natl. Acad. Sci. U.S.A.* **1999**, *96*, 6014–6019.
- (4) Spassky, A.; Angelov, D. *Biochemistry* **1997**, *36*, 6571–6576.
- (5) Angelov, D.; Spassky, A.; Berger, M.; Cadet, J. *J. Am. Chem. Soc.* **1997**, *119*, 11373–11380.
- (6) Burrows, C. J.; Muller, J. G. *Chem. Rev.* **1998**, *98*, 1109–1152.
- (7) Armitage, B. *Chem. Rev.* **1998**, *98*, 1171–1200.
- (8) Pogozelski, W. K.; Tullius, T. D. *Chem. Rev.* **1998**, *98*, 1089–1107.
- (9) O'Neill, P.; Parker, A. W.; Plumb, M. A.; Siebbeles, L. D. A. *J. Phys. Chem. B* **2001**, *105*, 5283–5290.
- (10) Henderson, P. T.; Jones, D.; Hampikian, G.; Kan, Y. Z.; Schuster, G. B. *Proc. Natl. Acad. Sci. U.S.A.* **1999**, *96*, 8353–8358.
- (11) Ly, D.; Sani, L.; Schuster, G. B. *J. Am. Chem. Soc.* **1999**, *121*, 9400–9410.
- (12) Kelley, S. O.; Holmlin, R. E.; Stemp, E. D. A.; Barton, J. K. *J. Am. Chem. Soc.* **1997**, *119*, 9861–9870.
- (13) Hall, D. B.; Holmlin, R. E.; Barton, J. K. *Nature* **1996**, *382*, 731–735.
- (14) Arkin, M. R.; Stemp, E. D. A.; Hormann, A.; Olson, E. J.; Barbara, P. F.; Barton, J. K. *Science* **1996**, *273*, 475–480.
- (15) Murphy, C. J.; Arkin, M. R.; Jenkins, Y.; Ghatlia, N. D.; Bossmann, S.; Turro, N. J.; Barton, J. K. *Science* **1993**, *262*, 1025–1029.
- (16) Cadet, J. *DNA adducts: Identification and significance*; Hemminki, K.; Dipple, A.; Shiker, D. E. F.; Kadlubar, F. F.; Segerback, D.; Bartsch, H., Eds.; IARC: Lyon, France, 1994.
- (17) O'Neill, M. A.; Barton, J. K. *Proc. Natl. Acad. Sci. U.S.A.* **2002**, *99*, 16543–16550.
- (18) O'Neill, M. A.; Barton, J. K. *J. Am. Chem. Soc.* **2002**, *124*, 13053–13066.
- (19) Livneh, E.; Tel-Or, S.; Elad, D.; Sperling, J. *Biochemistry* **1982**, *21*, 3698–3703.
- (20) Crespo-Hernández, C. E.; Arce, R. *J. Phys. Chem. B* **2003**, *107*, 1062–1070.
- (21) Ravanat, J. L.; Douki, T.; Cadet, J. *J. Photochem. Photobiol., B* **2001**, *63*, 88–102.
- (22) Kumar, S.; Davies, R. J. H. *Photochem. Photobiol.* **1987**, *45*, 571–579.
- (23) Bose, S. N.; Kumar, S.; Davies, R. J. H.; Sethi, S. K.; McCloskey, J. A. *Nucleic Acids Res.* **1984**, *12*, 7929–7947.
- (24) Bose, S. N.; Davies, R. J. H. *Nucleic Acids Res.* **1984**, *12*, 7903–7914.
- (25) Bose, S. N.; Davies, R. J. H.; Sethi, S. K.; McCloskey, J. A. *Science* **1983**, *220*, 723–725.
- (26) Zhao, X.; Taylor, J. S. *Nucleic Acids Res.* **1996**, *24*, 1561–1565.
- (27) Otoshi, E.; Yagi, T.; Mori, T.; Matsunaga, T.; Nikaido, O.; Kim, S. T.; Hitomi, K.; Ikenaga, M.; Todo, T. *Cancer Res.* **2000**, *60*, 1729–1735.
- (28) Zhao, X.; Kao, J. L.; Taylor, J. S. *Biochemistry* **1995**, *34*, 1386–1392.
- (29) Zhao, X.; Nadji, S.; Kao, J. L.; Taylor, J. S. *Nucleic Acids Res.* **1996**, *24*, 1554–1560.
- (30) Ballini, J. P.; Daniels, M.; Vigny, P. *Biophys. Chem.* **1991**, *39*, 253–265.
- (31) Crespo-Hernández, C. E.; Cohen, B.; Kohler, B. *Nature* **2005**, *436*, 1141–1144.
- (32) Crespo-Hernández, C. E.; Cohen, B.; Hare, P. M.; Kohler, B. *Chem. Rev.* **2004**, *104*, 1977–2019.
- (33) Crespo-Hernández, C. E.; Arce, R. *Photochem. Photobiol.* **2002**, *76*, 259–267.
- (34) Arce, R.; García, C.; Oyola, R.; Piñero, L.; Nieves, I.; Cruz, N. *J. Photochem. Photobiol., A* **2003**, *154*, 245–257.
- (35) García, C.; Oyola, R.; Piñero, L.; Cruz, N.; Alejandro, F.; Nieves, I.; Arce, R. *J. Phys. Chem. B* **2002**, *106*, 9794–9801.
- (36) Hatchard, C. G.; Parker, C. A. *Proc. R. Soc., Ser. A* **1956**, *235*, 518–536.
- (37) Johns, H. E. Quantum yields and kinetics of photochemical reactions in solution. In *Creation and detection of the excited state*; Lamola, A. A., Ed.; Marcel Dekker: New York, 1971; Vol. I, Part A, pp 123–172.
- (38) Crespo-Hernández, C. E.; Flores, S.; Torres, C.; Negrón-Encarnación, I.; Arce, R. *Photochem. Photobiol.* **2000**, *71*, 534–543.
- (39) Bryant, F. D.; Santus, R.; Grossweiner, L. I. *J. Phys. Chem.* **1975**, *79*, 2711–2716.
- (40) García, C.; Oyola, R.; Piñero, L.; Arce, R.; Silva, J.; Sánchez, V. *J. Phys. Chem. A* **2005**, *109*, 3360–3371.
- (41) Kolossvary, I.; Guida, W. C. *J. Comput. Chem.* **1993**, *14*, 691–698.
- (42) Crespo-Hernández, C. E.; Arce, R.; Ishikawa, Y.; Gorb, L.; Leszczynski, J.; Close, D. M. *J. Phys. Chem. A* **2004**, *108*, 6373–6377.
- (43) Steenken, S. *Chem. Rev.* **1989**, *89*, 503–520.
- (44) Deeble, D. J.; Das, S.; von-Sonntag, C. *J. Phys. Chem.* **1985**, *89*, 5784–5788.
- (45) Theard, L. M.; Peterson, F. C.; Myers, L. S., Jr. *J. Phys. Chem.* **1971**, *75*, 3815–3821.
- (46) Candeias, L. P.; Steenken, S. *J. Phys. Chem.* **1992**, *96*, 937–944.
- (47) Grabner, G.; Getoff, N.; Gantchev, Ts.; Angelov, D.; Shopova, M. *Photochem. Photobiol.* **1991**, *54*, 673–681.
- (48) Monti, S.; Köhler, G.; Grabner, G. *J. Phys. Chem.* **1993**, *97*, 13011–13016.
- (49) Sortino, S.; Scaiano, J. C. *Photochem. Photobiol.* **1999**, *70*, 590–595.
- (50) Buxton, G. V.; Greenstock, C. L.; Helman, W. P.; Ross, A. B. *J. Phys. Chem. Ref. Data* **1988**, *17*, 513–886.
- (51) O'Neill, P. *Radiat. Res.* **1983**, *96*, 198–210.
- (52) Steenken, S.; Vieira, A. J. S. C. *J. Phys. Chem.* **1987**, *91*, 4138–4144.
- (53) Arce, R. *Photochem. Photobiol.* **1987**, *45*, 713–722.
- (54) Crespo-Hernández, C. E.; Martínez, L.; González-Sierra, A. E.; Robles-Irizarry, L.; Díaz-Vázquez, A.; Arce, R. *J. Photochem. Photobiol., A* **2002**, *152*, 123–133.
- (55) Arce, R.; Martínez, L.; Danielsen, E. *Photochem. Photobiol.* **1993**, *58*, 318–328.
- (56) Crespo-Hernández, C. E.; Arce, R. *Photochem. Photobiol.* **2000**, *71*, 544–550.
- (57) Gidden, J.; Bowers, M. T. *Eur. Phys. J. D* **2002**, *20*, 409–419.
- (58) Seidel, C. A. M.; Schulz, A.; Sauer, M. H. M. *J. Phys. Chem.* **1996**, *100*, 5541–5553.
- (59) Fukuzumi, S.; Miyao, H.; Ohkubo, K.; Suenobu, T. *J. Phys. Chem. A* **2005**, *109*, 3285–3294.
- (60) Koning, T. M. G.; Davies, R. J. H.; Kaptein, R. *Nucleic Acids Res.* **1990**, *18*, 277–284.
- (61) We thank one of the reviewers for bringing this point to our attention.
- (62) Cárdenas, J. G. I.; Figueroa, K. A.; Vargas, C. V.; Gómez-Jeria, J. S.; Campos-Vallette, M. M. *Spectrosc. Lett.* **1988**, *23*, 107–125.
- (63) Markovitsi, D.; Onidas, D.; Gustavsson, T.; Lazzarotto, E. *J. Am. Chem. Soc.* **2005**, *127*, 17130–17131.
- (64) Close, D. M. *J. Phys. Chem. B* **2003**, *107*, 864–867.
- (65) Georgiou, S.; Bradrick, T. D.; Philippidis, A.; Beechem, J. M. *Biophys. J.* **1996**, *70*, 1909–1922.
- (66) Georgiou, S.; Kubala, S. M.; Large, C. C. *Photochem. Photobiol.* **1998**, *67*, 526–531.
- (67) Georgiou, S.; Gerke, L. S. *Photochem. Photobiol.* **1999**, *69*, 646–652.
- (68) Shih, C. C.; Georgiou, S. *J. Biomol. Struct. Dyn.* **2000**, *17*, 921–932.
- (69) Lewis, J. P.; Cheathan, T. E., III.; Starikov, E. B.; Wang, H.; Sankey, O. F. *J. Phys. Chem. B* **2003**, *107*, 2581–2587.
- (70) Bouvier, B.; Dognon, J.-P.; Lavery, R.; Markovitsi, D.; Millié, P.; Onidas, D.; Zakrzewska, K. *J. Phys. Chem. B* **2003**, *107*, 13512–13522.
- (71) Kuimova, M. K.; Cowan, A. J.; Matousek, P.; Parker, A. W.; Sun, X. Z.; Towrie, M.; George, M. W. *Proc. Natl. Acad. Sci. U.S.A.* **2006**, *103*, 2150–2153.